HHS Public Access

Author manuscript

Cell Rep. Author manuscript; available in PMC 2019 July 08.

Published in final edited form as:

Cell Rep. 2018 October 23; 25(4): 1018–1026.e4. doi:10.1016/j.celrep.2018.09.074.

Oncogenic R132 IDH1 Mutations Limit NADPH for *De Novo* Lipogenesis through (D)2-Hydroxyglutarate Production in Fibrosarcoma Cells

Mehmet G. Badur[1], **Thangaselvam Muthusamy**[1], **Seth J. Parker**[1], **Shenghong Ma**[2,3], **Samuel K. McBrayer**[4], **Thekla Cordes**[1], **Jose H. Magana**[1], **Kun-Liang Guan**[2,3], and **Christian M. Metallo**[1,3,5,*]

[1]Department of Bioengineering, University of California, San Diego, La Jolla, CA 92037, USA

[2]Department of Pharmacology, University of California, San Diego, La Jolla, CA 92037, USA

[3]Moores Cancer Center, University of California, San Diego, La Jolla, CA 92037, USA

[4]Department of Medical Oncology, Dana-Farber Cancer Institute and Harvard Medical School, Boston, MA 02115, USA

[5]Lead Contact

SUMMARY

Neomorphic mutations in NADP-dependent isocitrate dehydrogenases (*IDH1* and *IDH2*) contribute to tumorigenesis in several cancers. Although significant research has focused on the hypermethylation phenotypes associated with (D)2-hydroxyglutarate (D2HG) accumulation, the metabolic consequences of these mutations may also provide therapeutic opportunities. Here we apply flux-based approaches to genetically engineered cell lines with an endogenous *IDH1* mutation to examine the metabolic impacts of increased D2HG production and altered IDH flux as a function of *IDH1* mutation or expression. D2HG synthesis in *IDH1*-mutant cells consumes NADPH at rates similar to de novo lipogenesis. *IDH1*-mutant cells exhibit increased dependence on exogenous lipid sources for in vitro growth, as removal of medium lipids slows growth more dramatically in *IDH1*-mutant cells compared with those expressing wild-type or enzymatically inactive alleles. NADPH regeneration may be limiting for lipogenesis and potentially redox homeostasis in *IDH1*-mutant cells, highlighting critical links between cellular biosynthesis and redox metabolism.

In Brief

*Correspondence: cmetallo@ucsd.edu.

AUTHOR CONTRIBUTIONS

M.G.B., K.-L.G., and C.M.M. designed the study. M.G.B., T.M., S.J.P., S.M., S.K.M., T.C., and J.H.M. performed experiments and analyzed data. M.G.B. and C.M.M. wrote the manuscript. All authors read the manuscript.

DECLARATION OF INTERESTS

C.M.M. has previously consulted for Agios Pharmaceuticals.

SUPPLEMENTAL INFORMATION

Supplemental Information includes four figures and two tables and can be found with this article online at https://doi.org/10.1016/j.celrep.2018.09.074.

Badur et al. apply metabolic flux analysis to understand how oncogenic mutations in *IDH1* alter redox metabolism. Production of (D)2-hydroxyglutarate (D2HG) consumes NADPH at levels similar to de novo lipogenesis, and removal of lipids compromises *in vitro* growth of *IDH1*-mutant cells.

Graphical Abstract

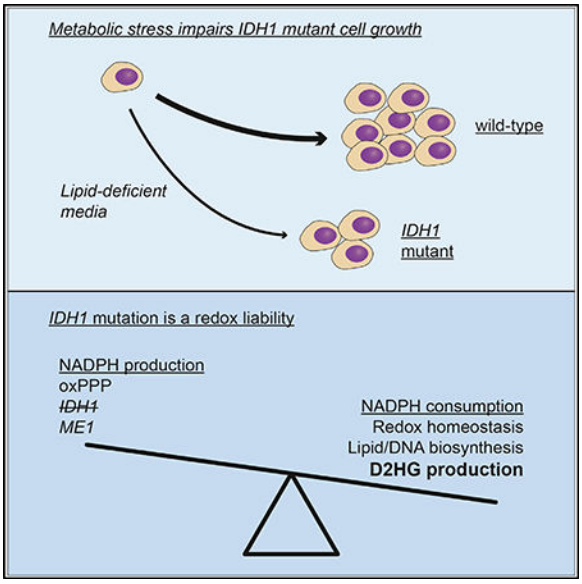

INTRODUCTION

Mutations in isocitrate dehydrogenase 1 (*IDH1*) and 2 (*IDH2*) are prevalent in acute myeloid leukemias, gliomas, sarcomas, and other tumors (Mardis et al., 2009; Parsons et al., 2008; Sjöblom et al., 2006; Yan et al., 2009). These gain-of-function mutations modify the activity of IDH1 and IDH2 such that the major reaction catalyzed is the NADPH-mediated reduction of a-ketoglutarate (aKG) to (D)2-hydroxyglutarate (D2HG) (Dang et al., 2009; Ward et al., 2010). In addition, mutant IDH1 and IDH2 exhibit decreased activity for the wild-type (WT) reaction, which reversibly interconverts isocitrate and NADP+ with aKG, CO_2, and NADPH (Ward et al., 2010). Therefore, cells harboring such IDH mutations exhibit metabolic reprogramming to compensate for these changes in enzyme activity.

Under hypoxic conditions, IDH1-mutant cells exhibit increased oxidative TCA flux, respiration, and decreased growth (Grassian et al., 2014). Although *IDH1*-mutant cells do not increase reductive carboxylation in hypoxia to the same extent as cells expressing only WT IDH1, mitochondrial metabolism and redox pathways are rewired to support the growth of mutant IDH1 cells in culture and *in vivo* (Carbonneau et al., 2016; Fack et al., 2017). More generally, IDH1-mutant cells exhibit various defects in mitochondrial metabolism, which may be therapeutically exploited by targeting NAMPT, BCL2, or other targets (Chan et al., 2015; Izquierdo-Garcia et al., 2015; Seltzer et al., 2010; Tateishi et al., 2015). These results demonstrate that *IDH1*-mutant cells exhibit similar metabolism to cells expressing

WT *IDH1* under basal conditions but altered metabolic states under conditions of bioenergetic or redox stress.

IDH1 is not thought to be a major source of NADPH in mammals (Fan et al., 2014). *IDH1*$^{-/-}$mice exhibit phenotypes only in select tissues or in response to specific stresses (i.e., nutrient deprivation) (Ye et al., 2017). In culture, overall IDH-mediated exchange flux is high, and the reverse reaction can support lipogenesis or compartment-specific redox maintenance in cancer cells under conditions of metabolic stress (Jiang et al., 2016; Metallo et al., 2011; Wise et al., 2011). The oxidative pentose phosphate pathway (oxPPP) is classically thought to be the primary pathway through which NADPH is regenerated in the cytosol (Stincone et al., 2015). Recent studies using ^{2}H tracing support this concept, whereby the oxPPP exhibits the highest contribution to cytosolic NADPH regeneration supporting biosynthesis(Zhang et al., 2016, 2017). Cell lines engineered to express mutant IDH1 enzymes exhibit increased oxPPP flux and differential lipid synthesis (Gelman et al., 2018), highlighting the importance of this pathway. On the other hand, knockout of oxPPP enzymes is particularly deleterious for cancer cell growth (Zhao et al., 2018).

To better understand how mutations in *IDH1* influence NADPH metabolism, we applied ^{13}C and ^{2}H metabolic flux analysis to an isogenic panel of fibrosarcoma cell lines that endogenously express IDH1$^{+/R132C}$ or were engineered to express a WT, R132C mutant, or enzymatically dead IDH1 enzyme after knocking out the original mutant allele (Ma et al., 2015). These cell lines recapitulate changes in anchorage-independent growth driven by mutant IDH1 (Ma et al., 2015) as well as the metabolic defects documented to occur under hypoxia. 2HG production and secretion were a major sink of NADPH in IDH1$^{+/R132C}$ cells, though cells could sufficiently compensate by modulating oxPPP flux. However, in lipid-deficient conditions D2HG production and secretion presented a metabolic liability that negatively affected *de novo lipogenic flux and in vitro* cell growth. These results demonstrate that IDH1 R132 mutations may be considered a significant redox liability in tumors, rendering them susceptible to metabolic stress.

RESULTS

Use of Genetically Engineered HT1080 Fibrosarcoma Cell Lines to Dissect Enzymatic Functions of IDH1 and Mutant IDH1

D2HG production in cells harboring R132 mutations in *IDH1* is dramatically increased and has an established role in tumorigenesis.Hereweinterrogatedredoxmetabolismoffibrosarcomacells using a genetically engineered panel of cell lines that recapitulate the metabolic reprogramming associated with oncogenic *IDH1* mutations. In this system, the mutant *IDH1* allele was knocked out of HT1080 fibrosarcoma cells (+/R132C), generating HT1080 cells heterozygous cell line for *IDH1* (+/-). Next, an isogenic IDH1-mutant panel was then re-expressed in the HT1080 *IDH1* (+/-) cell line generating vector control (PB; +/-), engineered WT *IDH1* (+/+), re-expressed *IDH1*-mutant (R132C; +/R132C), and catalytically dead double-mutant (T77A; +/R132C-T77A) cell lines (Ma et al., 2015). As depicted in Figure 1A, these cell lines exhibit distinct reprogramming of IDH1 enzymatic activity such that PB and WT cells maintain endogenous activity and do not readily produce D2HG, R132C mutants have reduced

endogenous IDH1 activity and produce D2HG, while T77A mutants have reduced endogenous IDH1 activity and do not accumulate D2HG(Maetal., 2015).Therefore,wecouldinterrogatethedistinct metabolic consequences of modulating WT IDH1 activity as well as neomorphic D2HG production by IDH1 R132C.

We first quantified per cell organic and amino acid abundances in each cell type, observing R132C-specific changes in abundance of glutamine and aKG (Figure 1B). In addition, we detected increased levels of non-essential amino acids (i.e., Glu, Ser, Pro, and Asp), consistent with previously described increases in glutaminolysis in *IDH1*-mutant cells (Grassian et al., 2014; Seltzer et al., 2010). We also observed elevated levels of Gly3P in R132C cells, suggesting that mitochondrial and/or cytosolic redox metabolism is perturbed in D2HG-producing cells (Figure 1B). On the other hand, intracellular abundance of most glycolytic metabolites, TCA metabolites, and other amino acids were not perturbed by altered IDH1 enzymatic function (Figure 1B). These results are consistent with general dispensability of IDH1 function in basal culture conditions.

Next, we characterized alterations in IDH flux in this isogenic fibrosarcoma cell line panel. Under conditions of hypoxia, IDH1 and IDH2 can support de *novo* lipogenesis by catalyzing the reductive carboxylation of aKG to isocitrate, which is subsequently metabolized to citrate and acetyl-coenzyme A (AcCoA) (Metallo et al., 2011). Cells harboring *IDH1* mutations are defective in their ability to convert glutamine carbon to citrate and AcCoA (Grassian et al., 2014). To this end, we cultured each HT1080 cell line in the presence of uniformly labeled ^{13}C glutamine ([U-$^{13}C_5$]glutamine) and quantified the isotopologue distribution of metabolites in central carbon metabolism (Figure 1C). We observed a significant decrease in M+5 citrate in R132C cells cultured in hypoxia compared with those expressing only functional WT IDH1, indicating that R132C-expressing cells were limited in their ability to generate citrate via reductive carboxylation (Figures 1D and S1A). We also observed a concomitant increase in M+4 citrate in R132C cells, consistent with previously described reliance of IDH1-mutant cells on oxidative glutaminolysis in hypoxia (Figures S1A and S1B; Grassian et al., 2014). We also observed altered labeling of aspartate from [U-$^{13}C_5$]glutamine that is consistent with decreased reductive carboxylation flux for generating cytosolic AcCoA (Figures 1E and S1C). This isogenic panel of HT1080 cells therefore recapitulates hallmarks of cancer cells expressing oncogenic IDH1 mutations. Notably, WT *IDH1* cells had the highest abundance of M+5 citrate and M+3 aspartate isotopologues, while PB and T77A cells (which have only one WT *IDH1* allele) had intermediate levels of these isotopologues (Figures 1D and 1E).

Cytosolic NADPH Contributes to D2HG Production from IDH1$^{+/R132C}$ Cells

Basal *IDH1* enzymatic function can facilitate both production and consumption of NADPH and is decreased in *IDH1*-mutant cells (Geisbrecht and Gould, 1999; Ward et al., 2010; Zhao et al., 2009), suggesting that cellular redox may be perturbed in these cells. To this end, we also observed elevated levels of Gly3P in R132C cells (Figure 1B). To investigate how redox metabolism is altered by IDH1 mutation, we cultured cells in the presence of [4-^{2}H]glucose and quantified enrichment on downstream metabolites (Figure 2A). This tracer specifically labels cytosolic NADH via GAPDH, and these deuterons are subsequently transferred to

lactate, malate, and Gly3P by downstream oxidoreductases (Lewis et al., 2014). We observed similar labeling in all cells tested (Figure 2B), indicating that no gross changes in NAD+ regeneration occurred upon perturbation of IDH1 activity.

We next examined how NADPH metabolism is altered in these HT1080 cell lines, as D2HG production by R132C IDH1 relies on the NADPH-dependent reduction of aKG. As NADPH and NADH pools are interconnected through transhydrogenase shuttles and enzymes (Cracan et al., 2017), the redox pathways that support 2HG production are not well understood. Indeed, D2HG accumulates to high millimolar intracellular concentrations in IDH-mutant cells (Dang et al., 2009), and we observed a drastic increase in intracellular 2HG only in R132C cells (Figure 2C). However, we also detected low levels of 2HG in cell lines expressing only WT IDH1 or enzymatically dead R132C-T77A IDH1 and hypothesized that L2HG was endogenously produced in these cells. To investigate the enantiomer of 2HG and source of reducing equivalents used for 2HG production in these cell lines, we cultured each cell type with [4-^{2}H]glucose or [3-^{2}H] glucose, which label NADH and NADPH respectively, and quantified 2HG labeling via gas chromatography-mass spectrometry (GC-MS) (Lewis et al., 2014). Results were distinct in that [4-^{2}H] glucose labeled approximately 10% of 2HG in PB, WT, and T77A cells, while [3-^{2}H]glucose labeled ~15% of 2HG in R132C cells (Figure 2D). These data suggest that L2HG is the predominant enantiomer present in cells expressing only WT IDH1, which has been demonstrated to be a byproduct of lactate dehydrogenase (LDH), malate dehydrogenase (MDH), or phosphoglycerate dehydrogenase (PHGDH) in cancer cells (Figure 2E; Fan et al., 2015; Intlekofer et al., 2015, 2017). Notably, 2HG enrichment from [3-^{2}H]glucose was similar to the expected enrichment of cytosolic NADPH calculated from fatty acid labeling (Figure 3C; Lewis et al., 2014). L2HG enrichment was significantly lower than that observed for lactate, malate, and Gly3P, suggesting that some 2HG is present in cells with WT IDH1. Ultimately, these results highlight the utility of deuterium tracing in assessing redox metabolism associated with altered IDH1 metabolism.

2HG Production Contributes Significantly to Cellular NADPH Demands

We next attempted to estimate how D2HG production and other pathways contribute to NADPH demands within cells by quantifying 2HG secretion flux. *De novo* lipogenesis (DNL) has been estimated to be the largest consumer of NADPH in cultured cells (Fan et al., 2014). We measured DNL flux for fatty acid and cholesterol synthesis using [1,2-$^{13}C_2$]glucose and isotopomer spectral analysis and compared the NADPH requirements for DNL and 2HG (Figure 3A). Strikingly, we found that the NADPH demand for D2HG production was relatively similar to that required for DNL (Figure 3A). Importantly, most D2HG-associated NADPH consumption was from the efflux of D2HG. This increased NADPH demand did not affect palmitate synthesis in R132C cells at early time points in culture (Figure S2A). However, we did observe an increased uptake of [^{13}C]palmitate from culture medium specifically in R132C cells, suggesting a potential reprogramming of lipid metabolism (Figure S2B).

We then asked if the consumption of NADPH by D2HG production influenced redox pathways associated with NADPH regeneration. The largest source of cytosolic NADPH in

cells is the oxPPP (Zhang et al., 2017). To probe any alterations in oxPPP redox function, we used a modeling approach to estimate the fraction of lipogenic NADPH supplied by the oxPPP (Figure 3B; Lewis et al., 2014). Despite the increased R132C-specific consumption of NAPDH by D2HG production, we found no change in the relative proportion of NADPH supplied by the oxPPP across these cell lines (Figure 3C). We also observed no alteration in the balance of flux (i.e., pathway activity) diverted to the oxPPP and non-oxPPP to both glycolytic intermediates (Figure S2C) and biomass-derived ribose (Figures S2D and S2E), indicating that cells were able to compensate for D2HG synthesis by increasing lipid uptake only.

To control for any clonal effects associated with production of the cell line panel, we then inhibited D2HG production in the parental HT1080 cell line using AGI-5198, a pharmacological inhibitor of mutant IDH1 (Rohle et al., 2013). We observed a~90% reduction in 2HG/aKG levels with AGI-5198 addition, implying a reduction in NADPH consumption by D2HG production (Figure 3D). However, inhibition of NADPH consumption did not alter NADPH supplied by oxPPP (Figure 3E). Taken together our data indicate that D2HG production does not alter the contribution of oxPPP flux to redox homeostasis, as cells are able to sufficiently rewire pathways to compensate for the increased NADPH demand. Indeed, we also quantified the contribution of oxPPP flux to lipogenic NADPH using engineered HCT116 cells with knockin of mutant *IDH1*. IDH1$^{+/R132H}$ HCT116 cells exhibited increased contributions of oxPPP to lipogenic NADPH pools (Figure 3F), highlighting the ability of cells to reprogram redox pathways to meet the increased demands for NADPH caused by oncogenic D2HG production.

DNL Competes with D2HG Production for NADPH

Our results suggest that R132C cells are able to compensate for NADPH consumed by D2HG production under normal growth conditions. However, this metabolic defect could become a liability in the context of altered nutrient conditions. Recent work has demonstrated the utility in altering extracellular nutrient conditions to understand cancer-specific metabolic liabilities and sparked an interest in engineering more physiologic media (Cantor et al., 2017). The tumor microenvironment is generally considered to be nutrient deficient, and tumor cells upregulate DNL to synthesize lipids necessary for growth (Ackerman and Simon, 2014). Indeed, lipogenesis is necessary for *in vitro* and *in vivo* tumor growth, and limitations in this pathway renders tumor cells more susceptible to chemotherapeutics (Svensson et al., 2016). To this end, we hypothesized that removal of exogenous lipids from cell culture media could alter R132C-specific growth by limiting the NADPH available for DNL flux. We observed that R132C cell growth was specifically decreased in delipidated culture conditions (Figure 4A). We also confirmed this growth phenotype in human oligodendroglioma (HOG) cells that ectopically express mutant IDH1 (Figures 4B and S3A). We then found that R132C cells exhibited decreased molar palmitate synthesis flux, suggesting the observed growth defect was mediated by an inability to synthesize enough lipids (Figure 4C).

We then asked what specific metabolic liability could be causing DNL defect in R132C cells. DNL is critical biosynthetic process that requires the coordination of many enzymes

and sufficient anabolic substrates (i.e., AcCoA and NADPH). As many possible factors could decrease DNL, we investigated potential drivers of this observed growth defect (Figure 4A). 2HG has been widely characterized as an inhibitor of aKG-dependent dioxygenase class enzymes that include important epigenetic modifiers (i.e., demethylases) (Figueroa et al., 2010; Lu et al., 2012; Turcan et al., 2012; Xu et al., 2011). We observed that expression of genes associated with fatty acid synthesis was not altered in R132C cells, implying that the production of D2HG, rather than a downstream epigenetic modification, caused the growth defect (Figure S3B). We also observed no alteration in the contribution of oxPPP flux to lipogenic NADPH, indicating that other redox pathways were not distinctly compensating (Figure S3C). We detected a slight increase in glucose contribution to lipogenic AcCoA, consistent with 2HG production shunting glutamine carbon away from DNL (Figure S3D). We also observed a concomitant increase in glutamine uptake in R132C cells cultured under delipidated conditions that could support 2HG production without limiting carbon for DNL (Figure S3D). Alterations in glutamine metabolism independent of 2HG production were observed in T77A double-mutant cells (Figure S3D), consistent with altered central carbon metabolite abundance (Figure S3E). Further work must be done to understand how loss of WT *IDH1* enzymatic activity reprograms metabolism to support DNL. Taken together, these changes are unlikely to account for the altered cell growth in delipidated conditions.

On the other hand, the desaturation index (C18:1/C18:0) quantified from total fatty acids in each cell line was significantly decreased in R132C cells (Figure 4D). Production of desaturated fatty acid species requires SCD activity, molecular oxygen, and NADPH (Kamphorst et al., 2013; Young et al., 2013). Because we did not detect changes in SCD expression (Figure S2B) and molecular oxygen is not limiting under normoxic conditions, this result suggests that NADPH was limiting R132C cells and could explain the decreased palmitate synthesis observed in R132C cells (Figure 4B). Importantly, we observed a dramatic increase in cholesterol biosynthesis with serum delipidation (Figure 4E). The NADPH requirements for cholesterol synthesis (26 molecules per cholesterol molecule) is a significant biosynthetic sink for NADPH, highlighting the importance of both fatty acid and sterol synthesis in contributing to the redox needs of proliferating cancer cells.

To better understand how NADPH regeneration fluxes were altered, flux through glycolysis and the oxPPP were quantified across the cell panel. We observed increased glycolytic fluxes in both R132C and T77A cells compared with WT (Figure 4F). Increased glycolytic flux is generally associated with altered mitochondrial state, but our data suggest that mitochondrial pathways are maintained by reprogramming of glutamine metabolism (Grassian et al., 2014). However, increased glucose uptake can also result in elevated oxPPP flux if branching is unchanged. We cultured cells in the presence of [1,2-^{13}C]glucose tracer to understand the relative shunting of glucose carbon through glycolysis and the oxPPP (Lee et al., 1998). We observed no difference in relative shunting to the oxPPP across the cell lines (Figure S2G). However, when combined with the increased glucose uptake and lactate efflux detected in R132C cells, these data indicate that oxPPP activity is significantly increased to meet the additional NADPH demands for D2HG production (Figure 4G). Importantly, R132C cells increase glucose uptake and oxPPP flux to a greater extent than T77A cells, implying that oxPPP flux and NADPH production is further increased to support

D2HG production (Figure 4G). In turn, the cells are unable to fully compensate for these NADPH demands and growth is reduced in lipid-deficient conditions.

Finally, we investigated whether pharmacological inhibition of 2HG production by AGI-5198 could alter growth in delipidated conditions. Administration of AGI-5198 *in vitro* did not improve growth under such conditions and slightly decreased cell growth (Figure S4A). Additionally, inhibition of 2HG production by AGI5198 did not alter the desaturation index of cellular fatty acids, suggesting that NADPH availability was not sufficiently altered (Figure S4B). As AGI-5198 does not completely block 2HG production at concentrations routinely used *in vitro* and could also inhibit WT enzyme activity (Figure 3D), further studies are needed to understand how inhibition of mutant IDH1 might influence the redox sensitivity of tumor cells in the context of combinatorial treatments.

DISCUSSION

The unique nature of IDH-mutant tumors has motivated a large research effort to identify potential targets within their signaling and metabolic networks (Chaumeil et al., 2013; Salamanca-Cardona et al., 2017; Turcan et al., 2018; Venteicher et al., 2017). The dramatic accumulation of 2HG in these tumors has focused much attention on the role of aKG-dependent dioxygenases in driving tumorigenesis (Losman and Kaelin, 2013). However, as IDH1 and IDH2 play critical roles in TCA metabolism and redox homeostasis, a greater understanding of the metabolic reprogramming required to support this unique liability may yield clues to additional therapeutic opportunities (Parker and Metallo, 2015). Such metabolic alterations could explain why genetic disruption of mutant *IDH1* affects the growth of some cells but not pharmacological inhibition (Jin et al., 2012, 2013).

Maintenance of redox homeostasis is essential for proper cell function, as pyridine nucleotides orthogonally connect bioenergetic and biosynthetic metabolic pathways (Badur and Metallo, 2018). Specifically, the regeneration of NADPH is required for anabolism of lipids, DNA, and proline as well as maintenance of reduced glutathione pools (Fan et al., 2014). However, the role of *IDH1* in the maintenance of redox homeostasis has been underappreciated. *IDH1* can functionally participate in a redox shuttle that interconnects mitochondrial and cytosolic NAD(P)H pools (Sazanov and Jackson, 1994). Indeed, this shuttle has been demonstrated to be critical for redox homeostasis in anchorage-independent conditions (Jiang et al., 2016). Upregulation of *IDH1* can promote the survival of pancreatic cancer cell lines under nutrient-limited conditions (Zarei et al., 2017). However, the largest source of NADPH in the cell is the oxPPP (Fan et al., 2014; Lewis et al., 2014; Zhang et al., 2017). Targeting of oxPPP enzymes is particularly deleterious to growth of cancer cell lines (Lin et al., 2015; Rao et al., 2015; Zhao et al., 2018), and coordinated therapeutic strategies that induce redox stress (e.g., nutrient modulation, radiation) while inhibiting pathways that promote redox homeostasis may be particularly effective (Conklin, 2004). Specifically, we highlight the importance of exogenous lipid availability in influencing cellular redox pathways, such that the increased NADPH requirements for fatty acid and sterol synthesis compromise growth of cell lines expressing mutant IDH1.

Our work suggests that IDH1-mutant tumor cells may be susceptible to therapeutic strategies that promote oxidative stress (albeit in cell culture); however, more extensive testing in animals is required to realize the translational potential of such approaches. We found that D2HG production is a major sink for NADPH, which is needed for reductive biosynthesis and redox homeostasis. When cells are challenged by lipid deficiency that drives cells to upregulate DNL flux, D2HG production becomes a metabolic liability that limits growth. Similar findings have recently been reported using engineered HCT116 cells (Gelman et al., 2018). Other pathways have also been described to compensate for such redox defects. For example, *IDH1* mutant glioma cells maintain redox homeostasis by enhancing the mitochondrial production of proline (Hollinshead et al., 2018). Metabolic profiling of low-grade gliomas has also correlated tumor progression with altered redox state (Jalbert et al., 2017). Additional studies are needed to understand if this redox sensitivity can be exploited in vivo. Recent work has demonstrated that D2HG can inhibit branched-chain amino acid transaminases (BCATs), compromising glutathione synthesis and sensitizing tumors to radiotherapy in combination with glutaminase inhibition (McBrayer et al., 2018). Such studies reinforce the concept that IDH mutations can reprogram the metabolic network to sensitize tumors to combinatorial therapies. Our studies highlight the importance of reducing equivalent availability in lipid biosynthesis. Although DNL is required for growth of lung tumors as xenografts or in genetically engineered mouse models (Svensson et al., 2016), the lipogenic requirements of sarcomas, gliomas, and other IDH1-mutant tumors may be different. Furthermore, the impact of dietary fat and combination therapies using mutant IDH1 inhibitors and/or radiation must be considered to appreciate the therapeutic potential of these findings. Nevertheless, our results highlight the impact of lipogenesis and D2HG production on cellular redox pathways.

STAR★METHODS

KEY RESOURCES TABLE

REAGENT or RESOURCE	SOURCE	IDENTIFIER
Chemicals, Peptides, and Recombinant Proteins		
[1,2-^{13}C]glucose	Cambridge Isotope Labs	CLM-504
[3-^{2}H]glucose	Omicron Biochemicals	GLC-034
[4-^{2}H]glucose	Omicron Biochemicals	GLC-035
[U-$^{13}C_6$]glucose	Cambridge Isotope Labs	CLM-1396
[U-$^{13}C_5$]glutamine	Cambridge Isotope Labs	CLM-1822
Critical Commercial Assays		
RNeasy Mini Kit	QIAGEN	74104
cDNA Reverse Transcription Kit	Thermo Fisher Scientific	4368814
Cyquant Cell Proliferation Assay	Thermo Fisher Scientific	C7026
Experimental Models: Cell Lines		
HCT116 parental and IDH1 knock-in clones (2H1, 2A9)	Horizon Discovery	N/A

REAGENT or RESOURCE	SOURCE	IDENTIFIER
HT1080	ATCC	N/A
HT1080 IDH1 panel	Ma et al. (2015)	https://doi.org/10.18632/oncotarget.3330
Human oligodendroma IDH1 panel	McBrayer et al. (2018)	https://doi.org/10.1016/j.cell.2018.08.038
Oligonucleotides		
RT-PCR primers, see Table S2	Primerbank	N/A
Software and Algorithms		
INCA	Young (2014)	https://mfa.vueinnovations.com/

CONTACT FOR REAGENT AND RESOURCE SHARING

Further information and requests for resources and reagents should be directed to and will be fulfilled by the Lead Contact, Christian Metallo (cmetallo@ucsd.edu).

EXPERIMENTAL MODEL AND SUBJECT DETAILS

Cell Lines and Culture Conditions—HT1080 and HCT116 cells were grown in DMEM supplemented with 10% FBS and 100 U/mL penicillin/streptomycin. HOG cells were grown in IMDM supplemented with 10% FBS, 100 U/mL penicillin/streptomycin, and 200 μg/mL hygromyocin (McBrayer et al.). HT1080 parental cells were obtained from ATCC. HCT116 parental and IDH1 knock-in clones (+/R132C; 2H1 and 2A9) were obtained from Horizon Discovery. Cells were maintained in humidified incubator at 5% CO_2. For hypoxia experiments, cells were maintained in humidified glove box (Coy) at 5% CO_2 and 1% O_2.

METHOD DETAILS

Cell growth and stable isotope tracing—For delipidated cell growth experiments, cells were plated in basal media. Fibrosarcoma cells were then allowed to adhere for 4 hours and then media was exchanged to delipidated media. HOG cells were allowed to adhere overnight and then media was exchanged to delipidated media. Cell growth was measured by either using hemocytometer for final cell counts or using Cyquant Cell Proliferation Assay (Molecular Probes) for estimation of DNA abundance, per manufacturer's protocol.

For isotopic labeling experiments, cells were plated in basal growth experiments and then rinsed with PBS before addition of tracing media. Cells were cultured in glucose- and glutamine-free media (GIBCO) supplemented with 10% dialyzed FBS, 100 U/mL penicillin/streptomycin, 4mM glutamine, and 25mM glucose. For glutamine tracing, cells were supplied ^{12}C glucose (Sigma) and [U-$^{13}C_5$]glutamine (99%, Cambridge Isotope Laboratories). For glucose tracing, cells were supplied ^{12}C glutamine (Sigma) and either [3-^{2}H]glucose (99%, Cambridge Isotope Laboratories), [4-^{2}H]glucose (99%, Omicron Biochemicals), [U-$^{13}C_6$] glucose (99%, Cambridge Isotope Laboratories), or [1,2-^{13}C]glucose (99%, Cambridge Isotope Laboratories). For palmitate uptake, [U-$^{13}C_{16}$]palmitate (99%, Cambridge Isotope Laboratories) was bound to fatty-acid free albumin (Roche) as previously described and supplied to cells at 50 μM (5% v/v) (Vacanti et

al., 2014). For delipidated tracing experiments, media was prepared in same way except using 10% dialyzed and delipidated FBS.

Delipidation of FBS—Normal or dialyzed FBS (GIBCO) was delipidated by first stirring 20 mg/mL fumed silica (Sigma) for 3 hr in ambient conditions. FBS slurry was then clarified by repeated centrifugation at 2000 g for 20 min. Supernatant was then sterile filtered (0.2 mm), aliquoted, and stored at −20C for future use.

Metabolite Extraction and GC-MS Analysis—Cells were rinsed with 0.9% (w/v) saline and 250 μL of —80^{O}C MeOH was added to quench metabolic reactions. 100 μL of ice-cold water supplemented with 10 μg/mL norvaline was then added to each well and cells were collected by scraping. The lysate was moved to a fresh 1.5 mL sample tube and 250 μL of —20^{O}C chloroform supplemented with 4 μg/mL D31 palmitate (and 4 μg/mL coprostan-3-ol if quantifying cholesterol) was added. After vortexing and centrifugation, the top aqueous layer and bottom organic layer were collected and dried under airflow. For analysis of cellular biomass, remaining interfacial layer was isolated, washed twice with methanol, and allowed to dried overnight with ambient airflow (Badur et al., 2015).

Derivatization of aqueous metabolites was performed using the Gerstel MultiPurpose Sampler (MPS 2XL). Methoxime- derivatives were formed by addition of 15 μL 2% (w/v) methoxylamine hydrochloride (MP Biomedicals) in pyridine and incubated at 45C for 60 minutes. Samples were then silylated by addition of 15 mL of N-tert-butyldimethylsily-N-methyltrifluoroacetamide (MTBSTFA) with 1% tert-butyldimethylchlorosilane (tBDMS) (Regis Technologies) and incubated at 45^{O}C for 30 minutes. Aqueous metabolites were analyzed by GC-MS using a DB-35MS column (30 m x 0.25mm i.d. x 0.25 mm, Agilent J&W Scientific, Santa Clara, CA) installed in an Agilent 7890B gas chromatograph (GC) interfaced with a 5977C mass spectrometer (MS). For separation of aqueous metabolites, the GC oven was held at 100^{O}C for 1 min after injection, increased to 255^{O}C at 3.5^{O}C/min, and finally increased to 320^{O}C at 15^{O}C/min and held for 3 min. Electron impact ionization was performed with the MS scanning over the range of 100–650 m/z.

Dried organic fraction was saponified and esterified to form fatty acid methyl esters (FAMEs) by addition of 500 μL of 2% (w/v) H_2SO_4 in MeOH and incubated at 50^{O}C for 120 minutes. FAMEs were then extracted by addition of saturated NaCl and hexane before collection and drying of the inorganic layer. Derivatized fatty acids were analyzed by GC-MS using a select FAME column (100 m x 0.25mm i.d. x 0.25 μm; Agilent J&W Scientific) installed in an Agilent 7890A gas chromatograph (GC) interfaced with a 5975C mass spectrometer (MS). For separation the GC oven was held at 80^{O}C for 1 min after injection, increased to 160^{O}C at 20^{O}C/min, increased to 198^{O}C at 1^{O}C/min, and finally increased to 250^{O}C at 5^{O}C/min and held for 15 min. Electron impact ionization was performed with the MS scanning over the range of 120–400 m/z. For cholesterol measurements, saponified organic phase was then redried under airflow and derivatized using a Gerstel autosampler by addition of 15 μL of N-methyl-N-trimethylsilyl-trifluoroacetamide (MSTFA; MachereyNagel) and incubated at 45^{O}C for 30 minutes. Cholesterol was was analyzed by GC-MS using a DB-35MS column (30 m x 0.25mm i.d. x 0.25 μm, Agilent J&W Scientific, Santa Clara, CA) installed in an Agilent 7890B gas chromatograph (GC) interfaced with a

5977C mass spectrometer (MS). For separation, the GC over was held at 150^{O}C for 1 min after injection, increased to 260^{O}C at 20^{O}C/min and held for 3 min, and then increased to 280^{O}C at 10^{O}C/min and held for 15 min. Electron impact ionization was performed with the MS scanning over the range of 70–800 m/z.

Cellular biomass was hydrolyzed with 2N HCl for 2 hr at 80^{O}C to release ribose monomers and then dried under airflow. Dried samples were then dissolved in 200 μL 2% (w/v) hydroxylamine hydrochloride in pyridine (Sigma) and incubated at 90C for 60 min. Next, 100 μL of propionic anhydride was added and samples were incubated at 60^{O}C for 30 min. Samples were then evaporated under airflow at 60^{O}C and resuspended in 100 μL ethyl acetate. Aldonitrile pentapropionate derivatives were then analyzed by GC-MS using a DB-35MS column (30 m x 0.25mm i.d. x 0.25 μm, Agilent J&W Scientific, Santa Clara, CA) installed in an Agilent 7890B gas chromatograph (GC) interfaced with a 5977C mass spectrometer (MS). For separation, the GC over was held at 100^{O}C for 1 min after injection and then increased to 255^{O}C at 20^{O}C/min and held for 4 min. Electron impact ionization was performed with the MS scanning over the range of 120–650 m/z.

Metabolite integration and isotopomer spectral analysis (ISA)—Isotopologue distributions and total abundances were determined by integration of mass fragments (Table S1) and correcting for natural abundances using in-house MATLAB-based algorithm.

Isotopomer spectral analysis (ISA) was performed to estimate contribution of oxPPP to cytosolic NADPH as previously described (Lewis et al., 2014). ISA compares experimental labeling of palmitate after 72 hr trace with [3-^{2}H]glucose to simulated labeling using a reaction network where C16:0 is condensation of 14 NADPHs. Parameters for contribution of *PGD* to lipogenic NADPH (D value) and percentage of newly synthesized fatty acid (g(t) value) and their 95% confidence intervals are then calculated using best-fit model from INCA MFA software (Young, 2014). Contribution of oxPPP was then estimated by doubling D value to account for stoichiometry of the oxPPP pathway.

Estimation of contribution of ^{13}C tracers to lipogenic AcCoA and palmitate synthesis was conducted as similar method to oxPPP contribution. Experimental fatty acid labeling from [U-$^{13}C_6$]glucose, [U-$^{13}C_5$]glutamine, or [1,2-^{13}C]glucose after 24–72 hr trace was compared to simulated labeling using a reaction network where C16:0 is condensation of 8 AcCoA. ISA data plotted as mean ± 95% CI. * indicates statistical significance by non-overlapping confidence intervals.

Estimation of cholesterol synthesis was similarly conducted. Experimental cholesterol labeling from [1,2-^{13}C]glucose or [U-$^{13}C_5$] glutamine after 24 hr trace was to compared to simulated labeling using a previously described reaction network (Kelleher et al., 1994). ISA data plotted as mean ± 95% CI.

Measurement of extracellular and intracellular fluxes—Initial and final concentrations of extracellular glucose, lactate, glutamine, and glutamate were determined by Yellow Springs Analyzer 2950 instrument. In parallel, cells were plated for initial and

final cell counts. Plated cells were pre-adapted to delipidated DMEM media for 24 hr before experiment.

The extracellular fluxes were described by the following differential equations:

$$\frac{dX}{dt} = \mu X$$

$$\frac{dN_i}{dt} = q_i X$$

$$\frac{dN_{gln}}{dt} = q_i X - kN_{gln}$$

where, X is concentration of cells, m is cellular growth (hr^{-1}), N is extracellular moles of metabolite i present, q_i is cell-specific consumption rate of metabolite i (mol/cell-hr), and k is first-order degradation rate of glutamine in cell culture (hr^{-1}). k was set to 0.0045 hr^{-1} as determined in literature (Tritsch and Moore, 1962).

Solution of ODEs yielded the following equations which we used to find extracellular fluxes:

$$X = X_0 e^{\mu t}$$

$$q_i = \frac{\mu\left(N_i - N_{i,0}\right)}{X - X_0}$$

$$q_{gln} = \frac{N_{gln} - N_{gln,0} e^{-kt}}{\left(\frac{1}{\mu + k}\right)\left(X - X_0 e^{-kt}\right)}$$

where subscript 0 signifies initial concentration.

For oxPPP measurement, glucose uptake measurement was coupled to ratio of (M1/(M1 + M2)) lactate label from [1,2-^{13}C] glucose tracer. This measurement is only appropriate when (1) considering relative differences across similar experimental conditions and (2) assuming that non-oxPPP flux and biosynthetic demands of ribose are not altered between conditions.

NADPH consumption—For fatty acid synthesis, consumption was defined as NADPH flux required to support biosynthesis of myristate (C14:0), palmitate (C16:0), stearate (C18:0), and oleate (C18:1) as these are predominantly synthesized species (Fan et al.,

2014). Cells were traced with [1,2-^{13}C]glucose for 24 hr and extracted for intracellular metabolites. In parallel, initial and final cell counts were taken. Per cell molar abundance of fatty acid species was determined by GC/MS. Percentage newly synthesized fatty acid was determined by ISA with reaction network where C14:0 is condensation of 7 AcCoA, C16:0 is condensation of 8 AcCoA, C18:0 is condensation of 9 AcCoA, and C18:1 is condensation of 9 AcCoA. Molar fatty acid synthesis flux was then calculated by dividing molar newly synthesized fatty acids by integral viable cell density over experimental time period. NADPH flux was then calculated by stoichiometric requirement of 12 NADPH per myristate, 14 NADPH per palmitate, 16 NADPH per stearate, and 17 NADPH per oleate.

For cholesterol, percentage newly synthesized was determined by ISA as stated above. Molar cholesterol synthesis flux was then calculated by dividing molar newly synthesized cholesterol by integral viable cell density over experimental time period. NADPH flux was then calculated by stoichiometric requirement of 26 NADPH per cholesterol.

For 2HG production fluxes, consumption was defined as NADPH flux required to support 2HG efflux and maintenance of intracellular abundance. Initial and final concentrations of extracellular 2HG were determined by GCMS analysis and use of external standard curves. Per cell molar abundance of 2HG was determined by GCMS at final time point. Efflux was then calculated similarly as above and dilutive flux was calculated by dividing intracellular concentration by specific growth rate. NADPH flux was then calculated by stoichiometric requirement of one NADPH per 2HG.

RT-PCR—Total mRNA was isolated from cells using RNA isolation kit (RNeasy Mini Kit; QIAGEN). Isolated RNA was reverse transcribed using cDNA synthesis kit (High-capacity cDNA Reverse Transcription Kit; Thermo Fisher Scientific). Real-time PCR was performed using SYBR green reagent (iTaq Universal SYBR Green Supermix; Bio-Rad). Relative expression was determined using Livak (ΔΔCT) method with *GAPDH* as housekeeping gene. Primers used were taken from Primerbank (Wang et al., 2012) and tabulated in Table S2. All commercial kits were used per the manufacturer's protocol.

QUANTIFICATION AND STATISTICAL ANALYSIS

Unless indicated, all results shown as mean ± SEM of biological triplicates. P values were calculated using a Student's two-tailed t test; *, P value between 0.01 and 0.05; **, P value between 0.001 and 0.01; ***, P value less than 0.001. Unless indicated, all normalization and statistical tests compared to WT cells.

Supplementary Material

Refer to Web version on PubMed Central for supplementary material.

ACKNOWLEDGMENTS

We are grateful William G. Kaelin Jr. for providing technical support and reagents. This work was supported by the California Institute of Regenerative Medicine (RB5–07356 to C.M.M.), the NIH (R01CA188652 to C.M.M. and R01CA196878 to K.-L.G.), a Camille and Henry Dreyfus Teacher-Scholar Award (to C.M.M.), and the National Science Foundation (NSF) Faculty Early Career Development (CAREER) Program (1454425 to C.M.M.). M.G.B. is supported by an NSF Graduate Research Fellowship (DGE-1144086).

REFERENCES

Ackerman D, and Simon MC (2014). Hypoxia, lipids, and cancer: surviving the harsh tumor microenvironment. Trends Cell Biol. 24, 472–478. [PubMed: 24985940]

Badur MG, and Metallo CM (2018). Reverse engineering the cancer metabolic network using flux analysis to understand drivers of human disease. Metab. Eng 45, 95–108. [PubMed: 29199104]

Badur MG, Zhang H, and Metallo CM (2015). Enzymatic passaging of human embryonic stem cells alters central carbon metabolism and glycan abundance. Biotechnol. J 10, 1600–1611. [PubMed: 26289220]

Cantor JR, Abu-Remaileh M, Kanarek N, Freinkman E, Gao X, Louissaint A Jr., Lewis CA, and Sabatini DM (2017). Physiologic medium rewires cellular metabolism and reveals uric acid as an endogenous inhibitor of UMP synthase. Cell 169, 258–272.e17. [PubMed: 28388410]

Carbonneau M, M Gagnè L, Lalonde ME, Germain MA, Motorina A, Guiot MC, Secco B, Vincent EE, Tumber A, Hulea L, et al. (2016). The oncometabolite 2-hydroxyglutarate activates the mTOR signalling pathway. Nat. Commun 7, 12700. [PubMed: 27624942]

Chan SM, Thomas D, Corces-Zimmerman MR, Xavy S, Rastogi S, Hong WJ, Zhao F, Medeiros BC, Tyvoll DA, and Majeti R (2015). Isocitrate dehydrogenase 1 and 2 mutations induce BCL-2 dependence in acute myeloid leukemia. Nat. Med 21, 178–184. [PubMed: 25599133]

Chaumeil MM, Larson PE, Yoshihara HA, Danforth OM, Vigneron DB, Nelson SJ, Pieper RO, Phillips JJ, and Ronen SM (2013). Non-invasive in vivo assessment of IDH1 mutational status in glioma. Nat. Commun 4, 2429. [PubMed: 24019001]

Conklin KA (2004). Chemotherapy-associated oxidative stress: impact on chemotherapeutic effectiveness. Integr. Cancer Ther 3, 294–300. [PubMed: 15523100]

Cracan V, Titov DV, Shen H, Grabarek Z, and Mootha VK (2017). A genetically encoded tool for manipulation of $NADP^+$/NADPH in living cells. Nat. Chem. Biol 13, 1088–1095. [PubMed: 28805804]

Dang L, White DW, Gross S, Bennett BD, Bittinger MA, Driggers EM, Fantin VR, Jang HG, Jin S, Keenan MC, et al. (2009). Cancer-associated IDH1 mutations produce 2-hydroxyglutarate. Nature 462, 739–744. [PubMed: 19935646]

Fack F, Tardito S, Hochart G, Oudin A, Zheng L, Fritah S, Golebiewska A, Nazarov PV, Bernard A, Hau AC, et al. (2017). Altered metabolic landscape in IDH-mutant gliomas affects phospholipid, energy, and oxidative stress pathways. EMBO Mol. Med 9, 1681–1695. [PubMed: 29054837]

Fan J, Ye J, Kamphorst JJ, Shlomi T, Thompson CB, and Rabinowitz JD (2014). Quantitative flux analysis reveals folate-dependent NADPH production. Nature 510, 298–302. [PubMed: 24805240]

Fan J, Teng X, Liu L, Mattaini KR, Looper RE, Vander Heiden MG, and Rabinowitz JD (2015). Human phosphoglycerate dehydrogenase produces the oncometabolite D-2-hydroxyglutarate. ACS Chem. Biol 10, 510–516. [PubMed: 25406093]

Figueroa ME, Abdel-Wahab O, Lu C, Ward PS, Patel J, Shih A, Li Y, Bhagwat N, Vasanthakumar A, Fernandez HF, et al. (2010). Leukemic IDH1 and IDH2 mutations result in a hypermethylation phenotype, disrupt TET2 function, and impair hematopoietic differentiation. Cancer Cell 18, 553–567. [PubMed: 21130701]

Geisbrecht BV, and Gould SJ (1999). The human PICD gene encodes a cytoplasmic and peroxisomal NADP(+)-dependent isocitrate dehydrogenase. J. Biol. Chem 274, 30527–30533. [PubMed: 10521434]

Gelman SJ, Naser F, Mahieu NG, McKenzie LD, Dunn GP, Chheda MG, and Patti GJ (2018). Consumption of NADPH for 2-HG synthesis increases pentose phosphate pathway flux and sensitizes cells to oxidative stress. Cell Rep. 22, 512–522. [PubMed: 29320744]

Grassian AR, Parker SJ, Davidson SM, Divakaruni AS, Green CR, Zhang X, Slocum KL, Pu M, Lin F, Vickers C, et al. (2014). IDH1 mutations alter citric acid cycle metabolism and increase dependence on oxidative mitochondrial metabolism. Cancer Res. 74, 3317–3331. [PubMed: 24755473]

Hollinshead KER, Munford H, Eales KL, Bardella C, Li C, Escribano-Gonzalez C, Thakker A, Nonnenmacher Y, Kluckova K, Jeeves M, et al. (2018). Oncogenic IDH1 mutations promote

enhanced proline synthesis through PYCR1 to support the maintenance of mitochondrial redox homeostasis. Cell Rep. 22, 3107–3114. [PubMed: 29562167]

Intlekofer AM, Dematteo RG, Venneti S, Finley LW, Lu C, Judkins AR, Rustenburg AS, Grinaway PB, Chodera JD, Cross JR, and Thompson CB (2015). Hypoxia induces production of L-2-hydroxyglutarate. Cell Metab. 22, 304–311. [PubMed: 26212717]

Intlekofer AM, Wang B, Liu H, Shah H, Carmona-Fontaine C, Rustenburg AS, Salah S, Gunner MR, Chodera JD, Cross JR, and Thompson CB (2017). L-2-hydroxyglutarate production arises from noncanonical enzyme function at acidic pH. Nat. Chem. Biol 13, 494–500. [PubMed: 28263965]

Izquierdo-Garcia JL, Viswanath P, Eriksson P, Cai L, Radoul M, Chaumeil MM, Blough M, Luchman HA, Weiss S, Cairncross JG, et al. (2015). IDH1 mutation induces reprogramming of pyruvate metabolism. Cancer Res. 75, 2999–3009. [PubMed: 26045167]

Jalbert LE, Elkhaled A, Phillips JJ, Neill E, Williams A, Crane JC, Olson MP, Molinaro AM, Berger MS, Kurhanewicz J, et al. (2017). Metabolic profiling of IDH mutation and malignant progression in infiltrating glioma. Sci. Rep 7, 44792. [PubMed: 28327577]

Jiang L, Shestov AA, Swain P, Yang C, Parker SJ, Wang QA, Terada LS, Adams ND, McCabe MT, Pietrak B, et al. (2016). Reductive carboxylation supports redox homeostasis during anchorage-independent growth. Nature 532, 255–258. [PubMed: 27049945]

Jin G, Pirozzi CJ, Chen LH, Lopez GY, Duncan CG, Feng J, Spasojevic I, Bigner DD, He Y, and Yan H (2012). Mutant IDH1 is required for IDH1 mutated tumor cell growth. Oncotarget 3, 774–782. [PubMed: 22885298]

Jin G, Reitman ZJ, Duncan CG, Spasojevic I, Gooden DM, Rasheed BA, Yang R, Lopez GY, He Y, McLendon RE, et al. (2013). Disruption of wild-type IDH1 suppresses D-2-hydroxyglutarate production in IDH1-mutated gliomas. Cancer Res. 73, 496–501. [PubMed: 23204232]

Kamphorst JJ, Cross JR, Fan J, de Stanchina E, Mathew R, White EP, Thompson CB, and Rabinowitz JD (2013). Hypoxic and Ras-transformed cells support growth by scavenging unsaturated fatty acids from lysophospholipids. Proc. Natl. Acad. Sci. U S A 110, 8882–8887. [PubMed: 23671091]

Kelleher JK, Kharroubi AT, Aldaghlas TA, Shambat IB, Kennedy KA, Holleran AL, and Masterson TM (1994). Isotopomer spectral analysis of cholesterol synthesis: applications in human hepatoma cells. Am. J. Physiol 266, E384–E395. [PubMed: 8166258]

Lee WN, Boros LG, Puigjaner J, Bassilian S, Lim S, and Cascante M (1998). Mass isotopomer study of the nonoxidative pathways of the pentose cycle with [1,2–13C2]glucose. Am. J. Physiol 274, E843–E851. [PubMed: 9612242]

Lewis CA, Parker SJ, Fiske BP, McCloskey D, Gui DY, Green CR, Vokes NI, Feist AM, Vander Heiden MG, and Metallo CM (2014). Tracing compartmentalized NADPH metabolism in the cytosol and mitochondria of mammalian cells. Mol. Cell 55, 253–263. [PubMed: 24882210]

Lin R, Elf S, Shan C, Kang HB, Ji Q, Zhou L, Hitosugi T, Zhang L, Zhang S, Seo JH, et al. (2015). 6-Phosphogluconate dehydrogenase links oxidative PPP, lipogenesis and tumour growth by inhibiting LKB1-AMPK signalling. Nat. Cell Biol 17, 1484–1496. [PubMed: 26479318]

Losman JA, and Kaelin WG Jr. (2013). What a difference a hydroxyl makes: mutant IDH, (R)-2-hydroxyglutarate, and cancer. Genes Dev. 27, 836–852. [PubMed: 23630074]

Lu C, Ward PS, Kapoor GS, Rohle D, Turcan S, Abdel-Wahab O, Edwards CR, Khanin R, Figueroa ME, Melnick A, et al. (2012). IDH mutation impairs histone demethylation and results in a block to cell differentiation. Nature 483, 474–478. [PubMed: 22343901]

Ma S, Jiang B, Deng W, Gu ZK, Wu FZ, Li T, Xia Y, Yang H, Ye D, Xiong Y, and Guan KL (2015). D-2-hydroxyglutarate is essential for maintaining oncogenic property of mutant IDH-containing cancer cells but dispensable for cell growth. Oncotarget 6, 8606–8620. [PubMed: 25825982]

Mardis ER, Ding L, Dooling DJ, Larson DE, McLellan MD, Chen K, Koboldt DC, Fulton RS, Delehaunty KD, McGrath SD, et al. (2009). Recurring mutations found by sequencing an acute myeloid leukemia genome. N. Engl. J. Med 361, 1058–1066. [PubMed: 19657110]

McBrayer SK, Mayers JR, DiNatale GJ, Shi DD, Khanal J, Chakraborty AA, Sarosiek KA, Briggs KJ, Robbins AK, Sewastianik T, et al. (2018). Transaminase inhibition by 2-hydroxyglutarate impairs glutamate biosynthesis and redox homeostasis in glioma. Cell 175, 101–116. [PubMed: 30220459]

Metallo CM, Gameiro PA, Bell EL, Mattaini KR, Yang J, Hiller K, Jewell CM, Johnson ZR, Irvine DJ, Guarente L, et al. (2011). Reductive glutamine metabolism by IDH1 mediates lipogenesis under hypoxia. Nature 481, 380–384. [PubMed: 22101433]

Parker SJ, and Metallo CM (2015). Metabolic consequences of oncogenic IDH mutations. Pharmacol. Ther 152, 54–62. [PubMed: 25956465]

Parsons DW, Jones S, Zhang X, Lin JC, Leary RJ, Angenendt P, Mankoo P, Carter H, Siu IM, Gallia GL, et al. (2008). An integrated genomic analysis of human glioblastoma multiforme. Science 321, 1807–1812. [PubMed: 18772396]

Rao X, Duan X, Mao W, Li X, Li Z, Li Q, Zheng Z, Xu H, Chen M, Wang PG, et al. (2015). O-GlcNAcylation of G6PD promotes the pentose phosphate pathway and tumor growth. Nat. Commun 6, 8468. [PubMed: 26399441]

Rohle D, Popovici-Muller J, Palaskas N, Turcan S, Grommes C, Campos C, Tsoi J, Clark O, Oldrini B, Komisopoulou E, et al. (2013). An inhibitor of mutant IDH1 delays growth and promotes differentiation of glioma cells. Science 340, 626–630. [PubMed: 23558169]

Salamanca-Cardona L, Shah H, Poot AJ, Correa FM, Di Gialleonardo V, Lui H, Miloushev VZ, Granlund KL, Tee SS, Cross JR, et al. (2017). In vivo imaging of glutamine metabolism to the oncometabolite 2-hydroxyglutarate in IDH1/2 mutant tumors. Cell Metab. 26, 830–841.e3. [PubMed: 29056515]

Sazanov LA, and Jackson JB (1994). Proton-translocating transhydrogenase and NAD- and NADP-linked isocitrate dehydrogenases operate in a substrate cycle which contributes to fine regulation of the tricarboxylic acid cycle activity in mitochondria. FEBS Lett. 344, 109–116. [PubMed: 8187868]

Seltzer MJ, Bennett BD, Joshi AD, Gao P, Thomas AG, Ferraris DV, Tsukamoto T, Rojas CJ, Slusher BS, Rabinowitz JD, et al. (2010). Inhibition of glutaminase preferentially slows growth of glioma cells with mutant IDH1. Cancer Res. 70, 8981–8987. [PubMed: 21045145]

Sjö blom T, Jones S, Wood LD, Parsons DW, Lin J, Barber TD, Mandelker D, Leary RJ, Ptak J, Silliman N, et al. (2006). The consensus coding sequences of human breast and colorectal cancers. Science 314, 268–274. [PubMed: 16959974]

Stincone A, Prigione A, Cramer T, Wamelink MM, Campbell K, Cheung E, Olin-Sandoval V, Grüning NM, Kruüger A, Tauqeer Alam M, et al. (2015). The return of metabolism: biochemistry and physiology of the pentose phosphate pathway. Biol. Rev. Camb. Philos. Soc 90, 927–963. [PubMed: 25243985]

Svensson RU, Parker SJ, Eichner LJ, Kolar MJ, Wallace M, Brun SN, Lombardo PS, Van Nostrand JL, Hutchins A, Vera L, et al. (2016). Inhibition of acetyl-CoA carboxylase suppresses fatty acid synthesis and tumor growth of non-small-cell lung cancer in preclinical models. Nat. Med 22, 1108–1119. [PubMed: 27643638]

Tateishi K, Wakimoto H, Iafrate AJ, Tanaka S, Loebel F, Lelic N, Wiederschain D, Bedel O, Deng G, Zhang B, et al. (2015). Extreme vulnerability of IDH1 mutant cancers to NAD+ depletion. Cancer Cell 28, 773–784. [PubMed: 26678339]

Tritsch GL, and Moore GE (1962). Spontaneous decomposition of glutamine in cell culture media. Exp. Cell Res 28, 360–364. [PubMed: 13994204]

Turcan S, Rohle D, Goenka A, Walsh LA, Fang F, Yilmaz E, Campos C, Fabius AW, Lu C, Ward PS, et al. (2012). IDH1 mutation is sufficient to establish the glioma hypermethylator phenotype. Nature 483, 479–483. [PubMed: 22343889]

Turcan S, Makarov V, Taranda J, Wang Y, Fabius AWM, Wu W, Zheng Y, El-Amine N, Haddock S, Nanjangud G, et al. (2018). Mutant-IDH1-dependent chromatin state reprogramming, reversibility, and persistence. Nat. Genet 50, 62–72. [PubMed: 29180699]

Vacanti NM, Divakaruni AS, Green CR, Parker SJ, Henry RR, Ciaraldi TP, Murphy AN, and Metallo CM (2014). Regulation of substrate utilization by the mitochondrial pyruvate carrier. Mol. Cell 56, 425–435. [PubMed: 25458843]

Venteicher AS, Tirosh I, Hebert C, Yizhak K, Neftel C, Filbin MG, Hovestadt V, Escalante LE, Shaw ML, Rodman C, et al. (2017). Decoupling genetics, lineages, and microenvironment in IDH-mutant gliomas by singlecell RNA-seq. Science 355, eaai8478. [PubMed: 28360267]

Wang X, Spandidos A, Wang H, and Seed B (2012). PrimerBank: a PCR primer database for quantitative gene expression analysis, 2012 update. Nucleic Acids Res. 40, D1144–D1149. [PubMed: 22086960]

Ward PS, Patel J, Wise DR, Abdel-Wahab O, Bennett BD, Coller HA, Cross JR, Fantin VR, Hedvat CV, Perl AE, et al. (2010). The common feature of leukemia-associated IDH1 and IDH2 mutations is a neomorphic enzyme activity converting alpha-ketoglutarate to 2-hydroxyglutarate. Cancer Cell 17, 225–234. [PubMed: 20171147]

Wise DR, Ward PS, Shay JE, Cross JR, Gruber JJ, Sachdeva UM, Platt JM, DeMatteo RG, Simon MC, and Thompson CB (2011). Hypoxia promotes isocitrate dehydrogenase-dependent carboxylation of a-ketoglutarate to citrate to support cell growth and viability. Proc. Natl. Acad. Sci. U S A 108, 19611–19616. [PubMed: 22106302]

Xu W, Yang H, Liu Y, Yang Y, Wang P, Kim SH, Ito S, Yang C, Wang P, Xiao MT, et al. (2011). Oncometabolite 2-hydroxyglutarate is a competitive inhibitor of α-ketoglutarate-dependent dioxygenases. Cancer Cell 19, 17–30. [PubMed: 21251613]

Yan H, Parsons DW, Jin G, McLendon R, Rasheed BA, Yuan W, Kos I, Batinic-Haberle I, Jones S, Riggins GJ, et al. (2009). IDH1 and IDH2 mutations in gliomas. N. Engl. J. Med 360, 765–773. [PubMed: 19228619]

Ye J, Gu Y, Zhang F, Zhao Y, Yuan Y, Hao Z, Sheng Y, Li WY, Wakeham A, Cairns RA, and Mak TW (2017). IDH1 deficiency attenuates gluconeogenesis in mouse liver by impairing amino acid utilization. Proc. Natl. Acad. Sci. U S A 114, 292–297. [PubMed: 28011762]

Young JD (2014). INCA: a computational platform for isotopically non-stationary metabolic flux analysis. Bioinformatics 30, 1333–1335. [PubMed: 24413674]

Young RM, Ackerman D, Quinn ZL, Mancuso A, Gruber M, Liu L, Giannoukos DN, Bobrovnikova-Marjon E, Diehl JA, Keith B, and Simon MC (2013). Dysregulated mTORC1 renders cells critically dependent on desaturated lipids for survival under tumor-like stress. Genes Dev. 27, 1115–1131. [PubMed: 23699409]

Zarei M, Lal S, Parker SJ, Nevler A, Vaziri-Gohar A, Dukleska K, Mambelli-Lisboa NC, Moffat C, Blanco FF, Chand SN, et al. (2017). Posttranscriptional upregulation of IDH1 by HuR establishes a powerful survival phenotype in pancreatic cancer cells. Cancer Res. 77, 4460–4471. [PubMed: 28652247]

Zhang H, Badur MG, Divakaruni AS, Parker SJ, Jäger C, Hiller K, Murphy AN, and Metallo CM (2016). Distinct metabolic states can support self-renewal and lipogenesis in human pluripotent stem cells under different culture conditions. Cell Rep. 16, 1536–1547. [PubMed: 27477285]

Zhang Z, Chen L, Liu L, Su X, and Rabinowitz JD (2017). Chemical basis for deuterium labeling of fat and NADPH. J. Am. Chem. Soc 139, 14368–14371. [PubMed: 28911221]

Zhao S, Lin Y, Xu W, Jiang W, Zha Z, Wang P, Yu W, Li Z, Gong L, Peng Y, et al. (2009). Glioma-derived mutations in IDH1 dominantly inhibit IDH1 catalytic activity and induce HIF-1alpha. Science 324, 261–265. [PubMed: 19359588]

Zhao D, Badur MG, Luebeck J, Magana JH, Birmingham A, Sasik R, Ahn CS, Ideker T, Metallo CM, and Mali P (2018). Combinatorial CRISPR-Cas9 metabolic screens reveal critical redox control points dependent on the KEAP1-NRF2 regulatory axis. Mol. Cell 69, 699–708.e7. [PubMed: 29452643]

Highlights

- D2HG production competes with reductive biosynthesis for NADPH in IDH1-mutant cells
- ^{2}H tracing resolves L2HG and D2HG production pathways
- IDH1 mutation slows cell growth when biosynthetic NADPH demands are increased

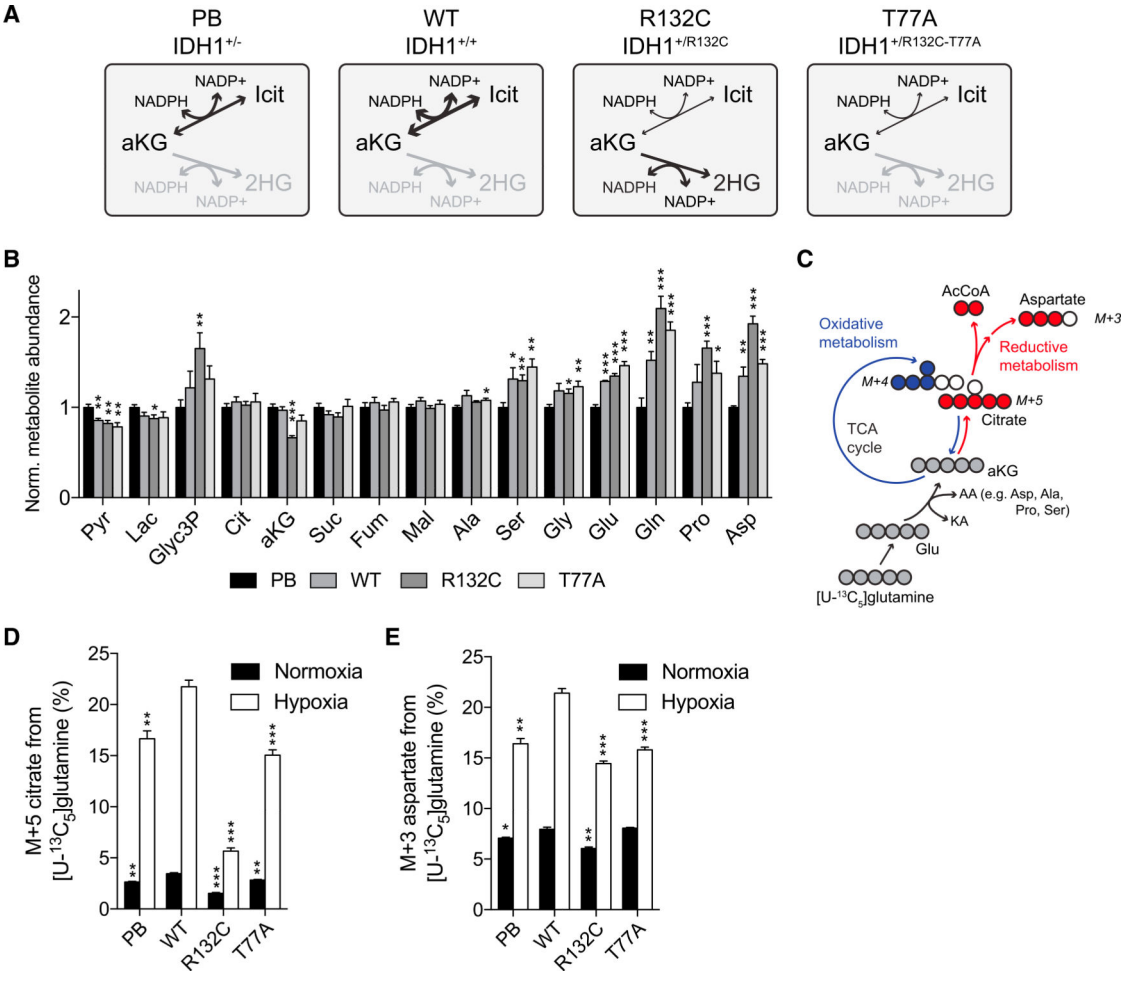

Figure 1. Metabolic Characterization of Isogenic IDH1-Expressing HT1080 Cell Lines

(A) Depiction of enzymatic activity present in each cell line.

(B) Relative intracellular abundance of glycolytic intermediates, TCA cycle metabolites, and amino acids (n = 6). Normalized to PB.

(C) Atom transition map of [U-$^{13}C_5$]glutamine for reductive and oxidative metabolism. Glutaminase and transamination of glutamate to aKG require concomitant amination of keto-acids (KA) to amino acids (AA) (e.g., Asp, Ala, Pro, Ser). Oxidative TCA flux leads to M+4 citrate. Reductive carboxylation of aKG leads to the M+5 citrate and subsequently M +3 aspartate.

(D) Percentage of M+5 citrate from [U-$^{13}C_5$]glutamine in normoxia and hypoxia.

(E) Percentage of M+3 aspartate from [U-$^{13}C_5$]glutamine in normoxia and hypoxia.

In (B), (D), and (E), data are plotted as mean ± SEM. Unless indicated, all data represent biological triplicates. See also Figure S1.

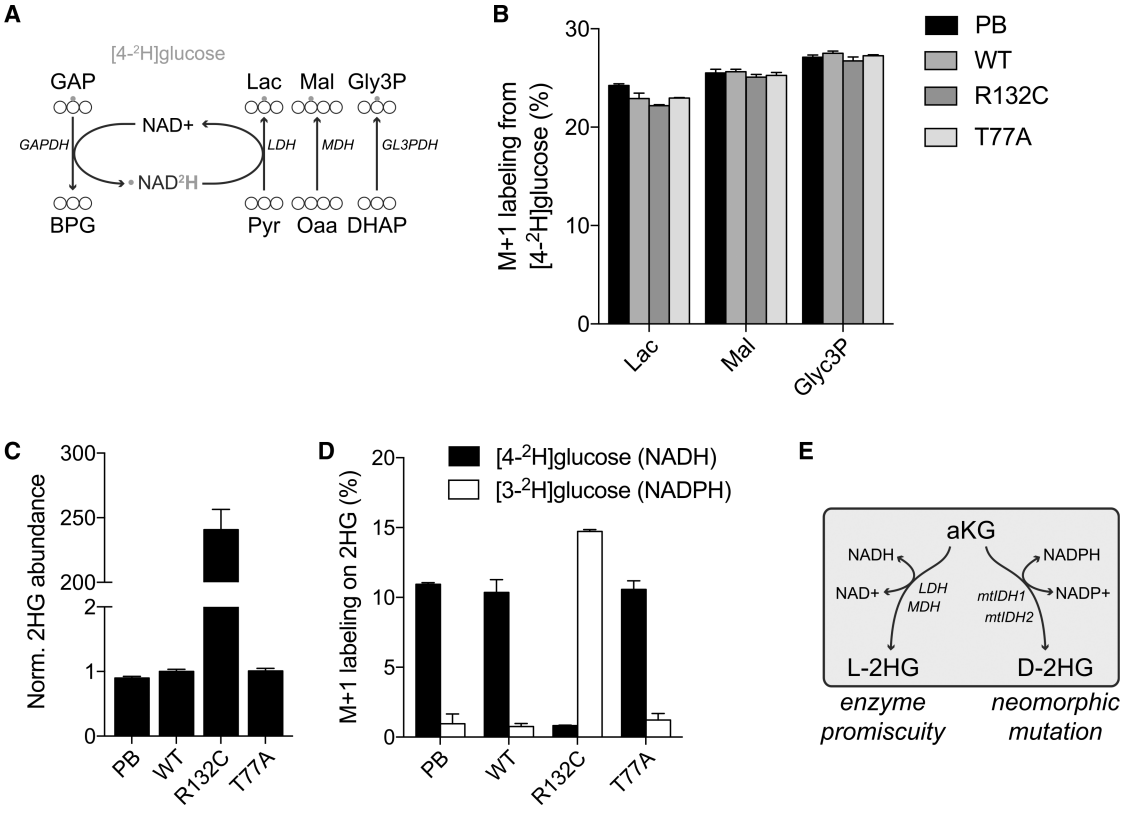

Figure 2. Tracing NAD(P)H Regeneration and 2HG Production in HT1080-IDH1 Cell Lines

(A) Atom transition map of [4-^{2}H]glucose. The tracer labels cytosolic NADH through GAPDH, leading to downstream labeling through lactate dehydrogenase (LDH), malate dehydrogenase (MDH), and glycerol-3-phosphate dehydrogenase (Gly3PDH).

(B) Percentage M+1 label from [4-^{2}H]glucose is not altered by *IDH1* status.

(C) Relative intracellular abundance of 2-hydroxyglutarate is increased in R132C cells.

(D) Percentage M+1 2HG label from [4-^{2}H]glucose and [3-^{2}H]glucose.

(E) Depiction of L2HG and D2HG production by NAD(P)H.

In (B)–(D), data are plotted as mean ± SEM. Unless indicated, all data represent biological triplicates.

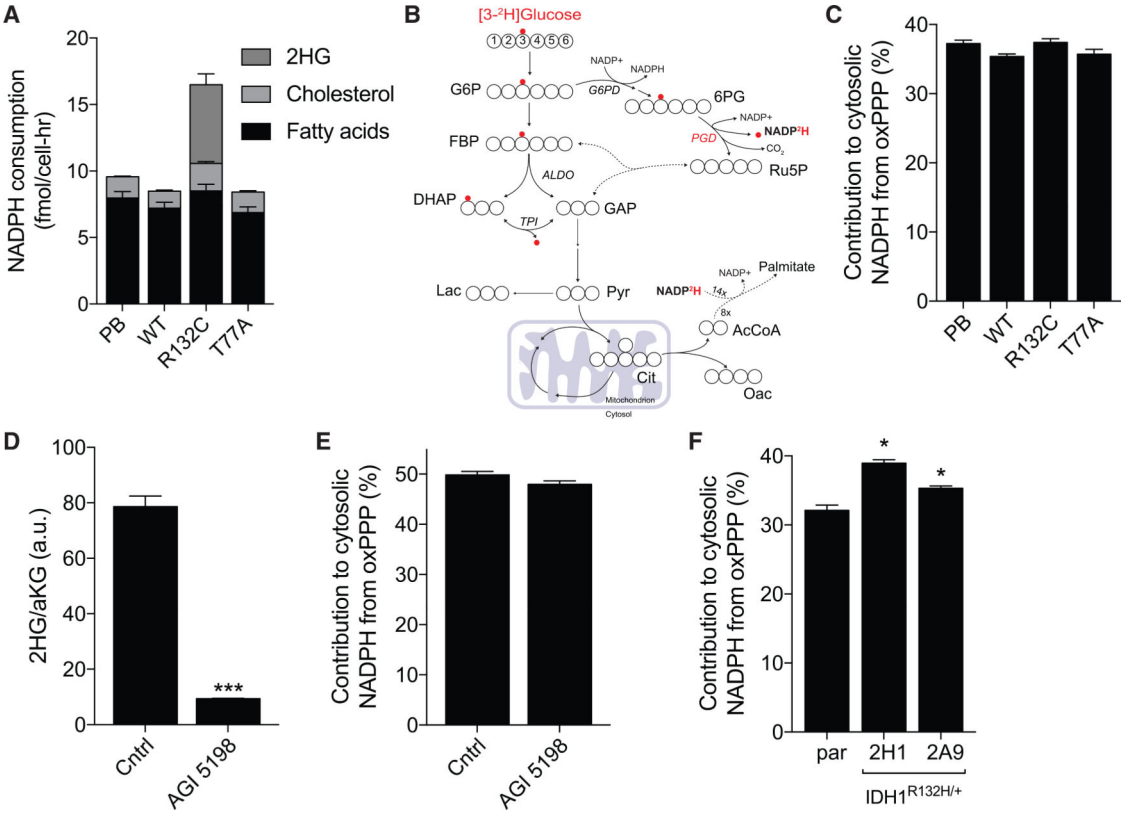

Figure 3. D2HG Production and Secretion Increase NADPH Demands in IDH1$^{+/R132C}$ Cells

(A) NADPH consumption fluxes by lipid synthesis and 2HG production in fibrosarcoma panel.

(B) Atom transition map of [3-^{2}H]glucose.

(C) Contribution of oxPPP to cytosolic NADPH in fibrosarcoma panel.

(D) 2HG abundance in parental HT1080 cells upon treatment with 10 mM AGI-5198.

(E) Contribution of oxPPP to cytosolic NADPH in parental HT1080 cells with 10 mM AGI-5198.

(F) Contribution of oxPPP to cytosolic NADPH in non-native IDH1-R132H engineered HCT116 cells.

In (A), (C), (E), and (F), data are plotted as mean ± 95% confidence interval (CI). *Statistical significance by non-overlapping confidence intervals. In (D), data are plotted as mean ± SEM. Unless indicated, all data represent biological triplicates. See also Figure S2.

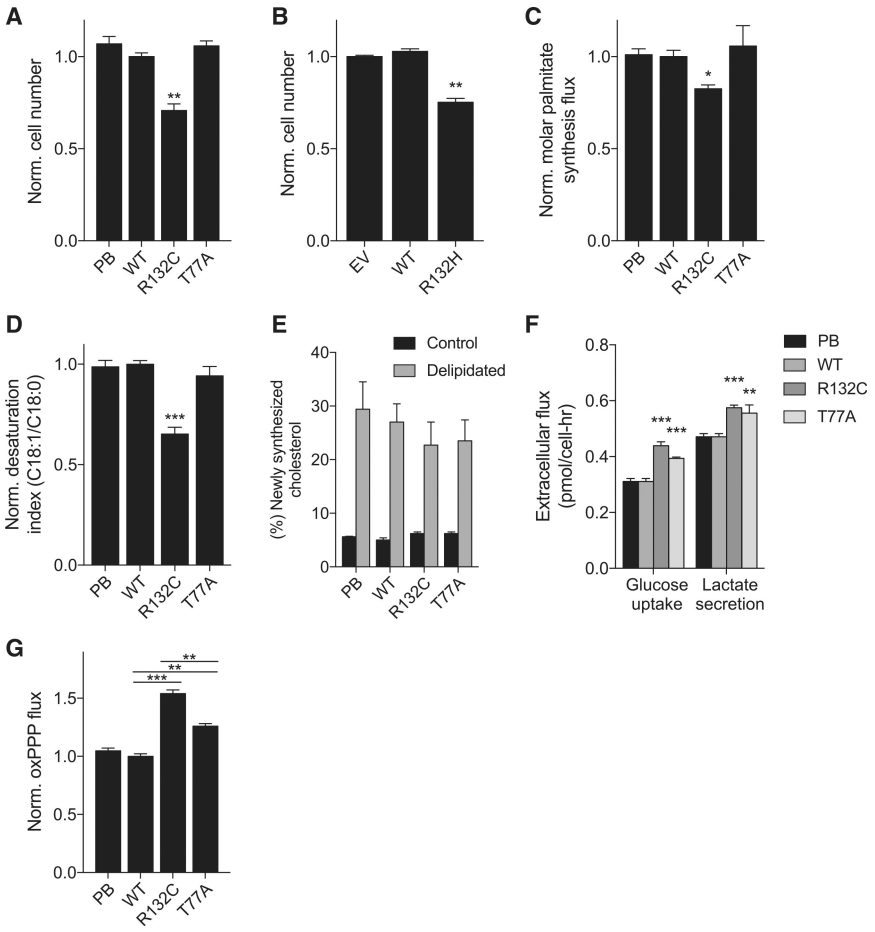

Figure 4. D2HG Production Limits NADPH for DNL in Lipid-Deficient Conditions

(A) Normalized cell number of fibrosarcoma panelafter 48 hr in delipidated conditions.

(B) Normalized cell number of HOG panel ectopically expressing *IDH1* after 96 hr in delipidated conditions.

(C) Normalized molar palmitate synthesis flux infibrosarcoma panel.

(D) Normalized desaturation index (C18:1/C18:0) in fibrosarcoma panel.

(E) Percentage newly synthesized cholesterol after24 hr in control or delipidated conditions in fibrosarcoma panel.

(F) Extracellular glucose uptake and lactate effluxin fibrosarcoma panel.

(G) Normalized oxPPP flux in delipidated conditions in fibrosarcoma panel.

In (A)–(D), (F), and (G), data are plotted as mean ± SEM. In (E), data are plotted as mean ± 95% CI. Unless indicated, all data represent biological triplicates. See also Figures S3 and S4.